Title
Coupling of radiation and hydrodynamics in a Z-pinch plasma

Journal
Journal of Applied Physics, 60(6)

ISSN
00218979

Authors
Bailey, J.
Fisher, A.
Rostoker, N.

Publication Date
1986

DOI
10.1063/1.337193

Peer reviewed

Coupling of radiation and hydrodynamics in a Z-pinch plasma

J. Bailey,[a] A. Fisher, and N. Rostoker
Department of Physics, University of California, Irvine, California 92717

(Received 13 January 1986; accepted for publication 14 May 1986)

The relationship between hydrodynamics and radiative energy loss from a gas puff Z pinch was studied using helium, krypton, and a helium–krypton mixture. The results show that radiation cooling enables the magnetic field to compress the plasma to a higher electron density and a smaller final radius. The data are consistent with a simple model describing the thermalization of the plasma on the axis of the pinch. The spectrum of the krypton radiation from the mixture was harder than from the pure krypton pinch. This may be important for application of the Z pinch as a radiation source.

I. INTRODUCTION

Radiation is an important energy loss mechanism for certain types of plasmas. If the radiation is sufficiently intense, it affects the other characteristics of the plasma, such as density, temperature, or size. The importance of this effect for a Z pinch was first suggested by Shearer.[1] In these experiments a gas puff Z pinch was used to investigate the role of radiative energy loss in determining the equilibrium conditions of a Z-pinch plasma.

A gas puff Z pinch is operated by injecting a hollow cylindrical gas shell into the space between two electrodes, then applying a high-voltage pulse to initiate a Z-pinch discharge. During the pinched stage, i. e., after the plasma shell begins to thermalize on axis but before instabilities cause disruption, the electron density reaches 10^{20} cm^{-3} and T_e is about 100 eV. This leads to ionization states of about 10 for argon or krypton. The energy radiated from a krypton plasma is typically 250 J, primarily in the ultrasoft (10 eV $< h\nu <$ 1 keV) x-ray region. The integrated radiation power approaches 10 GW, which is comparable to the rate at which the magnetic field does work on the plasma.

In the pinch, lighter atoms such as helium are completely ionized and emit relatively little radiation. Heavier atoms such as argon or krypton are only partially ionized so that many different bound–bound transitions are possible. These ions radiate copiously. Thus, qualitative conclusions concerning the importance of radiation can be drawn through comparison of plasmas containing low-Z ions with those of higher Z. It is difficult to draw any quantitative conclusions from this type of comparison, since the atomic mass may affect the initial jet conditions and compression dynamics. To avoid this complication we have compared a pure helium plasma to helium seeded with krypton. The objective is to add enough krypton to significantly enhance the radiation, but not enough to affect the implosion through the higher atomic mass of the krypton atoms. It has also been proposed[2,3] that radiation cooling could produce a population inversion through recombination into states with high quantum numbers, resulting in a soft x-ray laser.

With this goal in mind, measurements were made with plasmas containing pure krypton, pure helium, and a mixture of helium seeded with 1.5% krypton. The ultrasoft portion of the radiation was studied with an array of x-ray diodes. The column dynamics were determined with a pulsed nitrogen laser Mach–Zehnder interferometer. A dB/dt loop was used to monitor the current in the plasma column.

The data shows that the major effects of radiative energy loss are an increase in the maximum density and a smaller final radius. The experimental results are in agreement with a simple model. This model uses the energy balance equation to estimate the time resolved plasma temperature. The model shows that the measured radiation from the He–Kr mixture is sufficient to cause the temperature of the mixture plasma to increase more slowly than with a pure helium plasma. The magnetic field continues to compress the plasma until the temperature becomes high enough for the plasma pressure to balance the magnetic pressure. Thus, the slower temperature increase of the mixture plasma results in a smaller final radius.

II. EXPERIMENT

A. Apparatus

The University of California, Irvine, gas puff Z-pinch facility[4] was used to perform these experiments. A schematic drawing of the experimental geometry is shown in Fig. 1. The device consists of a stainless-steel cylindrical vacuum chamber. The cathode is mounted in one end plate and is separated from the vacuum chamber by an epoxy insulator. The anode consists of the top of a nozzle, mounted in the other end plate and held at ground potential. The annular nozzle is connected to an electromagnetic puff valve.[5] Rather than prefilling the chamber with gas, as in the traditional Z pinch, the fast electromagnetic valve is used to puff a cylindrical annulus of gas into the space between the two electrodes. After a preset delay (typically 100 μs) a voltage pulse is applied across the two electrodes, initiating a Z-pinch discharge. The return current is carried by the vacuum chamber walls.

The use of an initially hollow cylinder of gas allows the magnetic field to accelerate the plasma towards the axis without a significant increase in the plasma density. The current rise time is matched to the hydrodynamic compression time so that the actual compression of the plasma occurs when the current is close to its maximum. We can describe the pinch process more clearly if we divide the implosion

[a] Permanent address: Sandia Laboratories, Albuquerque, NM 87185.

 0021-8979/86/181939-07$02.40

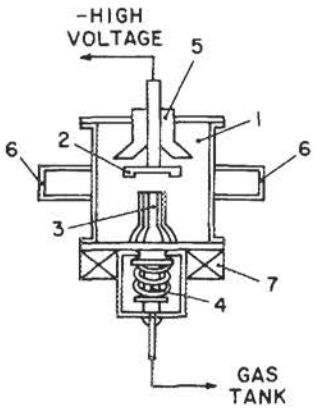

FIG. 1. Schematic diagram of the experimental geometry: (1) vacuum chamber, (2) cathode, (3) nozzle anode, (4) fast valve, (5) epoxy insulator, (6) diagnostic ports, (7) magnetic coil for fast valve. The interelectrode gap is 1 cm and the diameter of the annular nozzle is 4 cm.

into four stages: (1) injection of the gas followed by breakdown; (2) slow compression or run-in as the plasma column builds up kinetic energy; (3) thermalization in a uniform column on axis as the plasma kinetic energy is converted into thermal energy; and (4) disruption of the plasma column due to sausage and kink instabilities.

B. Diagnostics

The Mach–Zehnder interferometer used is described by Shiloh.[6] One interferogram can be taken on each discharge, giving us a snapshot of the plasma electron density as a function of radius. The time resolution is limited by the 5-ns length of the nitrogen laser pulse. To determine the electron density, cylindrical symmetry is assumed, permitting an Abel inversion of the fringe shift data. As the plasma approaches the axis the fringe shift is obscured by the higher density, the presence of large density gradients, and the motion of the plasma. The density is then estimated from the data obtained during the run-in stage of similar discharges, assuming conservation of mass. The accuracy of the final density is estimated to be $\pm$ 50%.

An array of ten x-ray diodes (XRDs) was used to measure the ultrasoft x-ray flux. This technique gives an absolute measurement of the radiation spectrum emitted between 20 eV and approximately 2 keV as a function of time. Its advantages are simplicity and low cost while providing good time resolution. The disadvantage is that we get only moderate energy resolution.

The diode sensitivity is a rapidly varying function of photon energy, so that we cannot learn much from the signal of a single XRD. However, when an array of diodes is used, each with a different spectral response, the power spectrum of the radiation can be determined. The basic deconvolution method is to iteratively determine the spectrum which yields the observed diode responses. Such a technique has been used successfully at several laboratories.[7–9] The deconvolution code used in this experiment was adapted from a routine developed by Degnan.[7]

A detailed discussion of the XRD measurement technique is given in Ref. 10. The absolute error is estimated to be $\pm$ 50%. The relative error is $\pm$ 10%.

A dB/dt loop was used to measure the current in the plasma column. This allows us to monitor the reproducibility of the discharge. Also, the rapid shrinking of the plasma radius as it nears the axis results in an increase in the plasma inductance. This appears as a sharp drop in dI/dt, providing a qualitative indication of the extent to which the plasma column is compressed.

III. RESULTS

A. Krypton

In this section we present the results obtained with pure krypton. The set of interferograms (Fig. 2) shows that the initial plasma column is hollow and exhibits no evidence of instabilities. The time given for each interferogram is with respect to the maximum ultrasoft x-ray intensity. The vertical line which appears in the center of all of the interferograms is the result of a scratch in one of the optical elements. From Abel inversions of the interferometer data, we estimate an electron line density of $N_e = 8\times10^{17}$/cm during the run-in. The ion line density, assuming $Z = 2$ during the run-in stage is $N_i = 4\times10^{17}$/cm. The assumption of $Z = 2$ is consistent with the lack of radiation emission during the run-in stage.

The outer radius of the column as a function of time (Fig. 3) was determined from the interferograms. The radius shown in Fig. 3 is an average taken along the length of the column. Each data point corresponds to a single interferogram. The smoothness of the curve formed by the data points indicates that the initial conditions and the time evolution of the current were highly reproducible, since variation in these two factors causes the radius reached at a given moment during the discharge to be different from shot to shot. The slope of the curve in Fig. 5 indicates that the column is compressed at a velocity of $1–2\times10^7$ cm/s. The minimum radius of the outer boundary of the column, $r = 0.06$ cm, was reached at about the same time as the peak in the

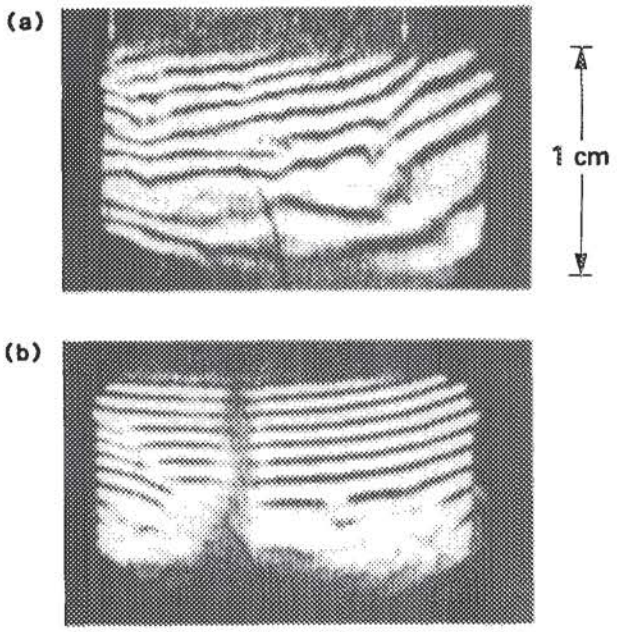

FIG. 2. Interferograms from krypton. The timing is with respect to the maximum ultrasoft x-ray emission. The arrows indicate the regions of highest density. (a) $t = -81$ ns, (b) $t = +9$ ns.

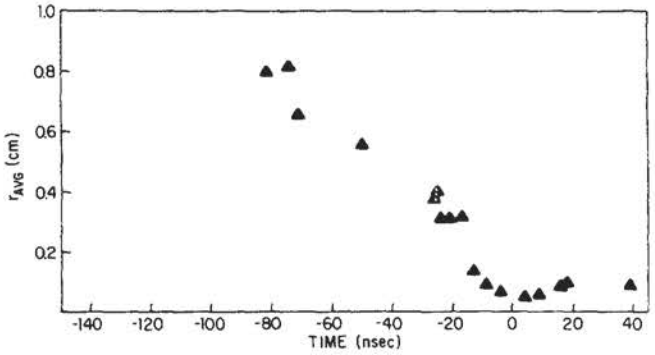

FIG. 3. Column radius as a function of time for krypton.

ultrasoft x-ray emission. The maximum ion density in the column was $n_i = 3.5\times10^{19}$ cm^{-3}. For $Z = 9$ (this ionization state is suggested by the XRD data and is consistent with data from other Z-pinch experiments),[11] we then have $n_e = 3.2\times10^{20}$ cm^{-3}.

A typical plot of the time-resolved ultrasoft x-ray emission is shown in Fig. 4. The integrated radiation power is shown in Fig. 5. Almost all of the emission occurs below $h\nu = 300$ eV. This is consistent with $n = 3$ to $n = 4$ transitions (n is the principal quantum number) in ionization states from Kr IX to Kr XIII.[12–15] According to the corona model,[16] a plasma temperature of about 100 eV is required to produce Kr IX–XIII.

B. Helium

A set of interferograms taken with pure helium is shown in Fig. 6. The helium ions fill the inside of the plasma shell during the run-in, so that the column does not remain hollow. On some discharges a diffuse cloud of plasma is present near the anode. The radial extent of this cloud is considerably larger than the radius of the rest of the column. The complicated structure of the fringe-shift data makes it difficult to measure the electron density. However, the fringe shift in Fig. 6(a) indicates an approximate electron line density of $N_e = 1.2\times10^{18}$/cm. The corresponding ion line density is $N_i = 6\times10^{17}$/cm, assuming $Z = 2$.

The outer radius of the plasma column as a function of time was determined from the interferograms (Fig. 7). The

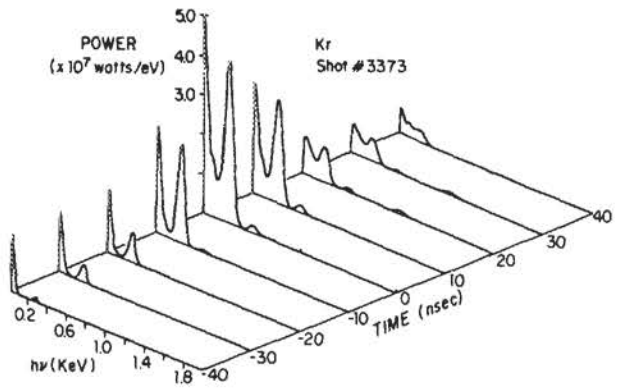

FIG. 4. Time resolved ultrasoft x-ray emission from krypton.

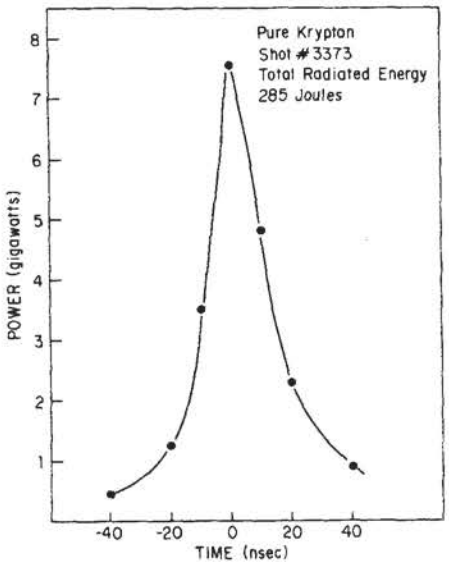

FIG. 5. Radiation power as a function of time for krypton, integrated over photon energy.

radius was averaged along the length of the column and the anode cloud was ignored in the measurement for Fig. 7. The radius approaches its minimum value of $r = 0.14$ cm [Fig. 6(c)] at a high velocity, $dr/dt = 2.8\times10^7$ cm/s. The maxi-

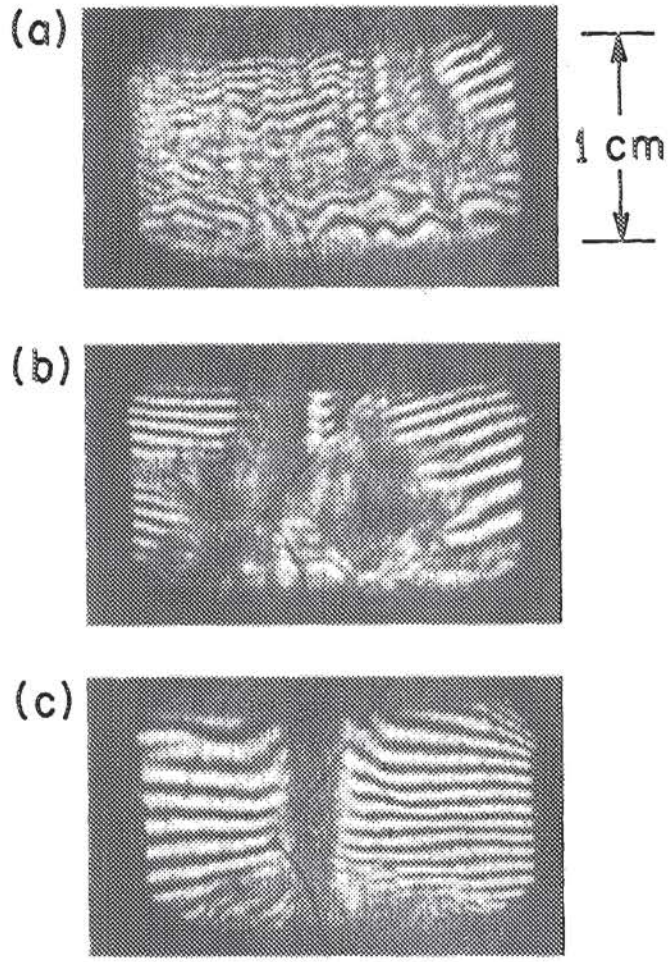

FIG. 6. Interferograms from helium. The timing is with respect to the sharp dip in dI/dt. (a) $t = -65$ ns, (b) $t = -18$ ns, (c) $t = -1$ ns.

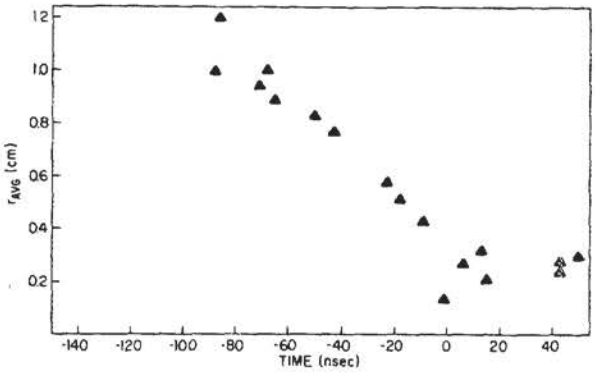

FIG. 7. Column radius as a function of time for helium.

mum electron density is $n_e = 1.9\times10^{19}$ cm^{-3}, with $n_i = 9.8\times10^{18}$ cm^{-3}.

The radiation from the pure helium was negligible. From the signal on the bare XRD (no signal was obtained on any of the filtered XRDs), we estimate the peak power radiated to be less than 0.5 GW.

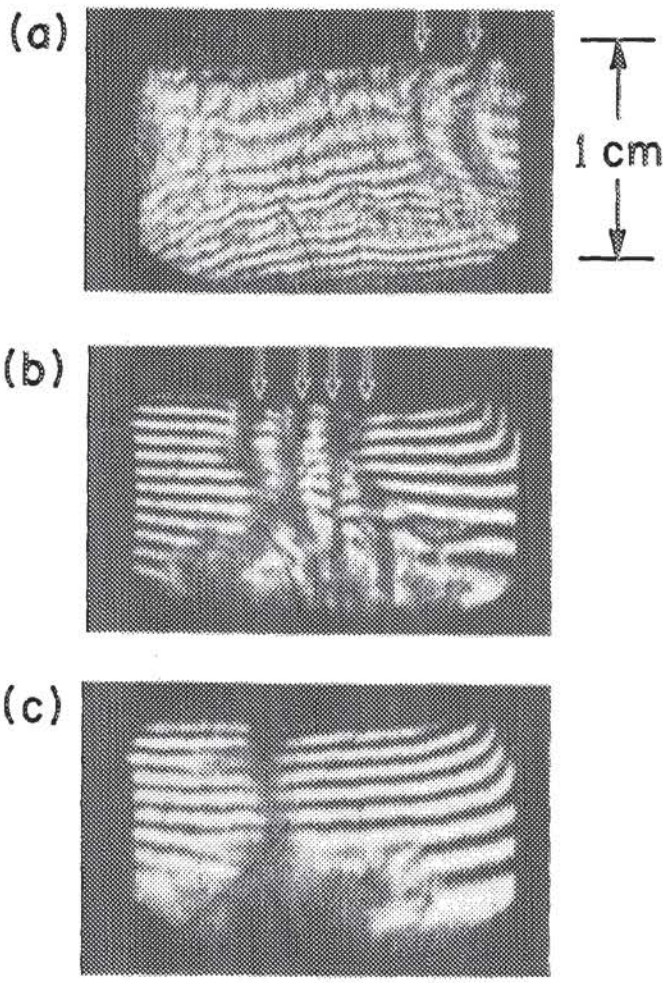

FIG. 8. Interferograms from the 98.5% He–1.5% Kr mixture. The timing is with respect to the maximum ultrasoft x-ray emission. The arrows indicate the regions of highest density. (a) $t = -74$ ns, (b) $t = -12$ ns, (c) $t = +2$ ns.

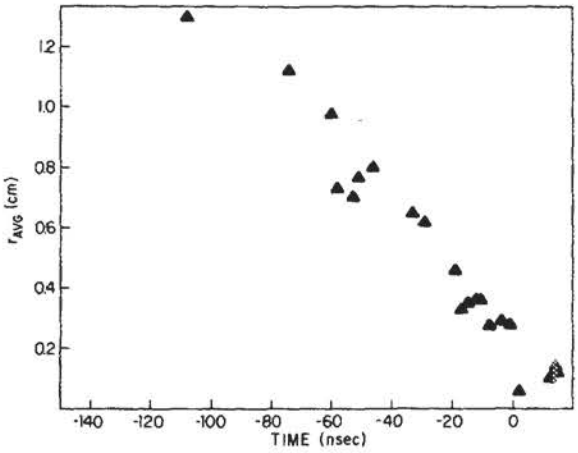

FIG. 9. Column radius as a function of time for the helium-krypton mixture.

C. Helium–krypton mixture

The helium–krypton mixture used was 98.5% He–1.5% Kr. The percentages are in terms of the number of atoms. The initial conditions were approximately the same as for pure helium. A set of interferograms from the mixture pinches is shown in Fig. 8. The separation effect previously observed in deuterium–argon mixtures[10,17] is evident here [Figs. 8(a) and 8(b)]. We interpret this phenomenon as a separation of atomic species due to their different atomic masses. Some of the helium ions run in ahead of the krypton ions. The conclusion that the observed phenomenon is a separation of atomic species is based on three facts: (1) With a high-Z gas, the annulus is hollow. (2) With a low-Z gas, some plasma fills the interior of the annulus prior to the collapse of the main plasma shell. (3) With some gas mixtures two distinct concentric shells are observed. As the relative percentage of the low-Z gas is increased, the amount of plasma found in the interior of the annulus increases.[10,17] Therefore, the inner shell is composed largely of the low-Z material. A model which explains these observations has been proposed by Barak and Rostoker.[18]

The axially averaged outer shell radius as a function of time was determined from the interferograms (Fig. 9). The cloud of plasma present near the anode was neglected in the radius measurements. The velocity prior to the final compression was $dr/dt = 2.6\times10^7$ cm/s, about the same as the implosion velocity of pure helium. The minimum value of the radius of the outer boundary of the outer shell was $r = 0.06$ cm, about a factor of 2 less than for pure helium.

Due to the high-density gradients and complicated structure of the fringe pattern, we were not able to directly measure the electron density in the mixture. However, since the initial conditions were close to those of pure helium, it is reasonable to assume that the number of ions in the mixture is about the same as the number of ions in the pure helium plasma. The ion line densities are then approximately the same. With this assumption, the total (He and Kr) ion line density in the mixture is $N_i = 6\times10^{17}$/cm. If the ion species are uniformly distributed throughout the plasma volume, then the maximum densities are $n_{He} = 5.3\times10^{19}$ cm^{-3} and

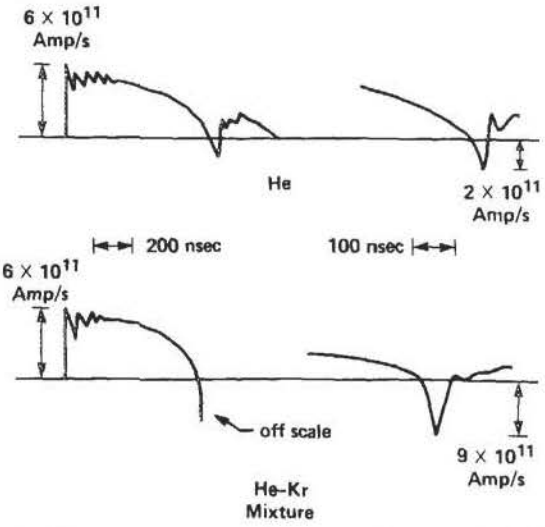

FIG. 10 Typical dI/dt signals from pure helium and the helium-krypton mixture. The dip which occurs at the pinch is shown on an expanded time scale.

$n_{Kr} = 2.7\times10^{17}$ cm^{-3}. The radiation data indicates that $Z_{Kr} = 9$. If we assume $Z_{He} = 2$ then the total average ionization state is $Z = 2.1$, and the maximum electron density is $n_e = 1.1\times10^{20}$ cm^{-3}. This is five times higher than the maximum electron density in the pure helium pinch.

The dip in dI/dt which occurs at the pinch is much more pronounced than for pure helium (Fig. 10). A larger drop in dI/dt corresponds to a larger change in the plasma inductance. This is further evidence that the mixture plasma is compressed to a smaller radius.

A typical time-resolved ultrasoft x-ray spectrum for the 98.5% He–1.5% Kr mixture is shown in Fig. 11. The integrated radiation power has the same time dependence as for pure krypton (Fig. 5), but the maximum value for the mixture is a factor of 2 lower. As in the pure Kr spectrum (Fig. 4), most of the emission occurs below $h\nu = 300$ eV, with peaks at 50 and 250 eV. However, there is some emission with $h\nu = 450$ eV and $h\nu = 1700$ eV. The 1700-eV radiation is consistent with line radiation from Kr XXVI–XXVII.

The 250-eV peak is twice as intense as the 50-eV peak. In the pure Kr spectrum the 250-eV peak was somewhat less intense than the 50-eV peak. For $\Delta n = 1$ transitions in this wavelength range, the wavelength of emitted photons becomes shorter as the atom is more highly ionized. Therefore, the average ionization state of the Kr atoms in the He–Kr mixture is higher than in the pure Kr plasma. This is supported by the presence of the radiation with $h\nu = 1700$ eV in the mixture data and not in the pure krypton data. It indicates that the spatially averaged plasma temperature may also be higher. An estimate for the electron temperature is 200 eV for the mixture compared to 100 eV for the pure krypton (Sec. IV).

The krypton atoms account for 25% of the total mass in the 98.5% He–1.5% Kr mixture. If the total mass is the same for the pure krypton pinch and the mixture, then the pure krypton pinch contains four times more krypton atoms. However, we know from the XRD measurement that the integrated radiation power from pure krypton is only a factor of 2 higher than from the mixture. Therefore, the power radiated per krypton ion in the mixture is about two times higher than in pure krypton. The mechanism which may be responsible for this phenomenon is collisional transfer of energy from helium ions to krypton ions. Spitzer's time scale[19] for temperature equilibration between the helium and krypton ions is about 0.1 ns. Thus, the kinetic energy carried by the helium ions is transferred to the krypton ions as the column is compressed on axis. This phenomenon may be useful for application of the Z pinch as a radiation source, since one is often interested in using only the harder (1 keV and above) portion of the spectrum.

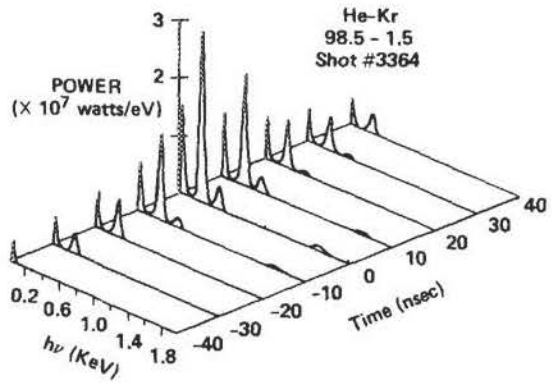

FIG. 11. Time-resolved ultrasoft x-ray emission from the helium–krypton mixture.

IV. DISCUSSION

In this section we discuss the results and show that radiation cooling can be significant compared to the other energy transfer mechanisms in a Z pinch. We first briefly describe the processes which affect the instantaneous power balance of the pinch. The terms in the power balance equation are then evaluated for the helium pinch. The thermal energy content of the helium plasma which is obtained from this analysis is used to estimate the plasma temperature as a function of time. The temperature of the mixture plasma is then obtained by subtracting the contribution of radiation cooling from the helium plasma thermal energy.

A. Introduction

During the compression, the azimuthal magnetic field does work on the plasma. The result of this work is an increase in the plasma kinetic energy. The plasma thermal energy does not become significant until the annular shell approaches pressure balance as it nears the axis. As the shell collapses on itself, the plasma kinetic energy is converted through collisional processes into thermal energy. The thermal energy of the plasma can also be increased through Ohmic heating. The compression is brought to a stop when the kinetic pressure of the plasma is comparable to the magnetic pressure. If moderate atomic number atoms (e. g., krypton) are present, the increase in plasma temperature results in high ionization states and copious emission of line radiation. The resulting radiative energy loss can reduce the rate of increase in the plasma temperature, permitting enhanced compression of the plasma.

B. Power balance equation

The power balance can be expressed as

$$\frac{dE_K}{dt} = \frac{dW}{dt} - P_{KT}\,,$$
$$\frac{dE_{\rm th}}{dt} = P_{KT} + P_\Omega - P_R\,, \tag{1}$$

where E_K = plasma kinetic energy, dW/dt = the rate at which the magnetic field does work on the plasma, P_{KT} = the rate at which plasma kinetic energy is transferred to thermal energy, $E_{\rm th}$ = plasma thermal energy, P_Ω = the rate of Ohmic heating, and P_R = the rate of radiative energy loss.

The rate of work by the magnetic field can be written as[1]

$$\frac{dW}{dt} = P\frac{dV}{dt} = \frac{I^2}{10^5}\frac{\dot r}{r}\ \ (\mathrm{W})\,, \tag{2}$$

where P is the magnetic pressure, V is the plasma volume, I is the current in amps, and r is the outer radius of the plasma in cm.

A lower bound on the classical Ohmic heating rate can be obtained by assuming that the current is uniformly distributed throughout the plasma and estimating the average plasma temperature from the Bennett equilibrium relation. When the pinch reaches equilibrium, the estimate is $T = 100$ ev for pure krypton and $T = 200$ eV for both pure helium and the helium–krypton mixture. The electron and ion temperatures are approximately equal, since the time scale for equilibration of the electron and ion temperatures is shorter than the column lifetime. Using Spitzer's resistivity, we find that the Ohmic heating rate of the helium plasma is $P_\Omega = 0.2$ GW when the plasma reaches its minimum radius. Since this is much less than P_{KT}, we can neglect Ohmic heating in a first-order solution of the power balance equation.

The next term to evaluate is the rate for converting kinetic to thermal energy. Using the relaxation rate approach,[20] the decrease in the plasma kinetic energy during a small time interval of the collisional thermalization is given by

$$P_{KT} = \frac{E_K(t_0)}{\tau}e^{-\Delta t/\tau}\,, \tag{3}$$

where $E_K(t_0)$ is the kinetic energy at the beginning of the small time interval, $\Delta t = 5$ ns is the length of the time interval, and τ is the constant for the decay.

In order to use this expression, we need to evaluate the time constant τ. When the inner radius of the hollow shell reaches the axis, the collision rate between plasma particles first undergoes a local increase in the vicinity of the axis and a shock propagates radially outward. The effective speed at which the shock front moves outward is approximately equal to the sum of the column velocity (2×10^7 cm/s) and the hydromagnetic wave speed (1×10^7 cm/s). The time scale for the information that the shell has reached the axis to propagate through the plasma (τ_s) is the annular thickness divided by the effective shock speed. For our experiments, τ_s is about 20 ns.

After this shock front has passed through a region of the plasma, the particles in the region behind the front begin to thermalize. The Spitzer[19] time scales for a single species to relax to a Maxwellian distribution and for temperature equilibration of different species were found to be smaller than τ_s. Thus, we conclude that τ_s, the time for the shock front to propagate out to the boundary of the plasma, is the dominant time scale governing the thermalization process.

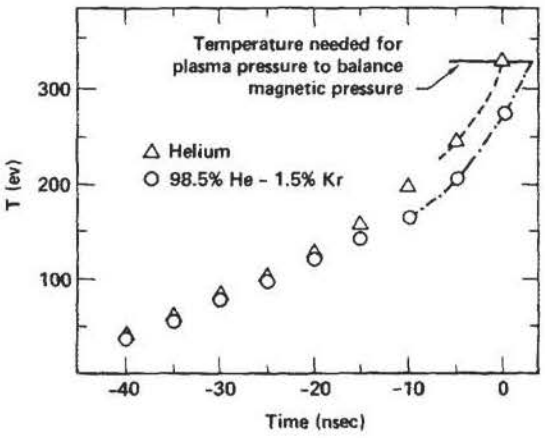

FIG. 12. Estimated average plasma temperature as a function of time. The curves were obtained from the power balance equation.

C. Results of the power balance analysis

A rough estimate of the helium plasma temperature at the beginning of the thermalization ($t = 45$ ns) is $T = 5$ eV. The average ionization state is assumed constant at $Z = 2$. The initial kinetic energy is estimated to be 20 J from the plasma velocity and mass. The temperature obtained from the power balance is shown in Fig. 12. The maximum temperature of the helium pinch is $T = 300$ eV. This is about 50% higher than the temperature derived from the Bennett equilibrium.

The terms in the power balance equation for the mixture are the same as for helium except for the radiation cooling term. The estimate for the mixture plasma temperature, obtained by subtracting the measured radiation energy from the thermal energy of the helium plasma, is shown in Fig. 12. About 15 ns before maximum compression, the radiation increases sharply. Until this time the temperatures for the two gases are about the same. When the radiative energy loss from the mixture increases, the rate of increase in the plasma temperature slows. At the point where the helium plasma reaches its maximum temperature and minimum radius, the temperature in the 98.5% He–1.5% Kr mixture is 50 eV lower, so that the mixture plasma has insufficient kinetic pressure to balance the magnetic field. From Fig. 12, an additional 2.5 ns elapse before the mixture reaches equilibrium. During this time the plasma is being compressed at a velocity of approximately 2.8×10^7 cm/s. This corresponds to an additional 0.07-cm change in the plasma radius, beyond the radius at which the helium plasma reaches equilibrium. Subtracting this additional change from the minimum radius of the helium pinch, the model predicts a minimum radius of $r\sim0.07$ cm for the mixture. This is in excellent agreement with the experimentally determined value.

V. CONCLUSIONS

We have shown that adding a small amount of krypton to helium has a major effect on the pinch dynamic and x-ray spectrum. The pinch is hotter than pure krypton and the final pinch diameter is smaller than the pure helium pinch. The x-ray spectrum measurements and the interferograms are consistent with the assumption that the heating is due to conversion of kinetic energy to thermal energy and Ohmic heating can be neglected.

ACKNOWLEDGMENT

This work has been supported by the Department of Energy at Sandia Laboratories.

[1]J. W. Shearer, Phys. Fluids **19**, 1426 (1976).
[2]M. H. Key, Nature **316**, 314 (1985).
[3]S. Suckewer and H. Fishman, J. Appl. Phys. **51**, 1922 (1980).
[4]J. Shiloh, A. Fisher, and N. Rostoker, Phys. Rev. Lett. **40**, 515 (1978).
[5]A. Fisher, F. Mako, and J. Shiloh, Rev. Sci. Instrum. **49**, 872 (1978).
[6]J. Shiloh, Ph.D. thesis, University of California, Irvine, 1978.
[7]J. Degnan, R. J. Sand, G. F. Kuittu, and D. M. Woodall, in *Low Energy X-Ray Diagnostics, Proceedings of the Conference at Monterey, 1981* (American Institute of Physics, New York, 1981), p. 264.
[8]R. H. Day, P. Lee, E. B. Saloman, D. J. Nagel, "X-Ray Diodes for Laser Fusion Plasma Diagnostics," Los Alamos Scientific Laboratory Report LA-7941-MS (1981).
[9]E. J. T. Burns, Adv. X-Ray Anal. **18**, 117 (1974).
[10]J. Bailey, Ph.D. thesis, University of California, Irvine, 1984.
[11]R. E. Marrs, D. D. Dietrich, M. A. Levine, D. F. Price, R. E. Stewart, and B. K. F. Young, Appl. Phys. Lett. **42**, 946 (1983).
[12]L. A. Jones and E. Kallne, "A Study of the VUV Emission from Highly Ionized Krypton in a Theta Pinch Plasma," Center for Astrophysics Preprint No. 1780 (1982).
[13]M. W. D. Mansfield, N. J. Peacock, C. C. Smith, M. G. Hobby, and R. D. Cowan, J. Phys. B **11**, 1521 (1978).
[14]R. D. Bleach, J. Opt. Sci. Am. **70**, 861 (1980).
[15]R. Stewart (private communication).
[16]D. E. Post, R. V. Jensen, C. B. Tarter, W. H. Grasberger, and W. A. Lokke, At. Data Nucl. Data Tables **20**, 397-439 (1977).
[17]J. Bailey, Y. Ettinger, A. Fisher, and N. Rostoker, Appl. Phys. Lett. **40**, 460 (1982).
[18]G. Barak and N. Rostoker, Appl. Phys. Lett. **41**, 918 (1982).
[19]L. Spitzer, *Physics of Fully Ionized Gases* (Wiley, New York, 1962).
[20]S. Glasstone and R. H. Lovberg, *Controlled Thermonuclear Reactions* (Krieger, Huntington, NY, 1960), pp. 99–100.